

High resolution spectroscopy and spectral simulation of C_2 using degenerate four-wave mixing

G. M. Lloyd and P. Ewart

Clarendon Laboratory, University of Oxford, Parks Road, Oxford OX1 3PU, United Kingdom

(Received 14 August 1998; accepted 30 September 1998)

Degenerate four-wave mixing in the sub-Doppler phase conjugate geometry was used to record high resolution spectra of the $d\ ^3\Pi_g - a\ ^3\Pi_u$ (0-0) Swan band of C_2 produced in an oxy-acetylene flame. The line positions of isolated transitions were measured to an accuracy of $\sim 3 \times 10^{-3} \text{ cm}^{-1}$ and calibrated using a Fizeau interferometer system. The data obtained from these spectra was used to calculate rotational constants and lambda doubling parameters for the $^3\Pi$ states from which the line positions for the whole band were calculated. Noticeable improvements between experimental and calculated line positions are seen when compared to previously published values. The effect of inaccuracies in line positions on the simulation of degenerate four-wave mixing spectra is discussed and some examples of the improvement in simulation using the newly calculated line positions are presented. © 1999 American Institute of Physics. [S0021-9606(99)03701-0]

I. INTRODUCTION

Spectroscopic study of radical or transient species such as excited or chemically reactive molecules is often hampered by the hostile conditions in which such species are created. Typical environments include flames and plasmas operated over a wide range of temperature and pressure where the high luminosity limits the signal to noise ratio of spectra and resolution is often degraded by the Doppler effect. Laser techniques such as laser-induced fluorescence (LIF) and nonlinear optical methods providing coherent signals, offer solutions to some of these experimental problems. The nonlinear processes of degenerate four-wave mixing (DFWM), and polarization spectroscopy (PS) have been shown to allow high resolution spectroscopy of molecular or radical species in flames.^{1,2} In particular DFWM has been used for a variety of measurements in combustion and plasma diagnostics³ and is finding increasing application in studies of molecular dynamics.⁴ Quantitative interpretation of spectra requires a detailed understanding of the signal generation process and their accurate simulation in turn requires accurate values of relevant molecular parameters. The aim of the present paper is to show that DFWM may be used for high resolution spectroscopy of molecular radicals to determine accurate absolute values of electronic transition wavelengths leading to improved values of the molecular constants. The accurate and precise wavelength determination is vital for synthesis of complex molecular spectra where spectral features may consist of two or more unresolved components. In the case of spectra generated by nonlinear methods such as DFWM the correct prediction of spectral intensities is critically dependent on the relative positions of unresolved components owing to the coherent addition of their respective contributions. The importance of these considerations is illustrated in the present work by a study of the DFWM spectrum of C_2 .

Recent interest in the C_2 radical reflects its importance in combustion and plasma chemistry as well as astrophysics.

LIF has been used to detect the radical in flames⁵ and to measure absolute concentrations in a flame⁶ and a low pressure plasma.⁷ Polarization spectroscopy has also been used to generate Doppler broadened spectra⁸ by scanning a narrow bandwidth dye laser. Broadband or multiplex spectra were recorded using DFWM in single laser shots and used to derive time-resolved temperature values in an oxy-acetylene flame.⁹ More recently DFWM with counterpropagating pump beams was used in our laboratory to yield sub-Doppler spectra for comparison with simulated spectra derived using the published line positions in the (0-0) band of the $d\ ^3\Pi_g - a\ ^3\Pi_u$ system of C_2 .¹⁰ In this previous work the spectra were recorded using laser intensities which were considered to be just below saturation levels. From the present work it is clear that partial saturation was present in the previously presented spectra. This is evident in the previous work where broadening of the spectral lines and reduced resolution was observed in regions where the spectrum becomes congested. It was noted that some spectral features showed apparently higher resolution than the corresponding theoretical simulation. This phenomenon was ascribed to the effects of interference arising from coherent addition where contributions from closely spaced lines led to destructive interference. This effect also is enhanced by the broadening caused by partial saturation and will be explored further in a separate publication.¹¹ It was noted that the quality of spectral simulation depended critically on the accuracy of spectral line positions in constructing features consisting of several unresolved components. The relative intensity of strongly blended features is an important aspect of the simulation if the spectra are to be used as probes of the local environment, e.g., for inferring a flame temperature. Although it was apparent that inaccuracies in transition wavelengths could affect the simulation the spectral resolution obtained in the previous work was insufficient to make a meaningful test of published spectral line positions.

In this paper we report the use of DFWM to obtain high

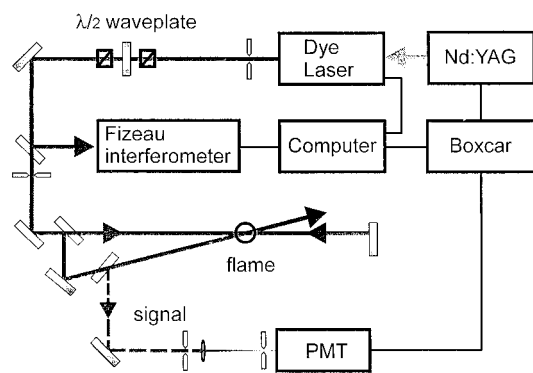


FIG. 1. Schematic diagram of the experimental set-up.

resolution spectra of the $(0-0) d^3\Pi_g-a^3\Pi_u$ band of C_2 produced in an atmospheric pressure oxy-acetylene flame. Special care was taken to ensure the spectra were unsaturated in order to avoid line broadening. Spectral simulation using the most accurate values of the transition frequencies obtained using Fourier transform spectroscopy by Amiot¹² and by Prasad and Bernath¹³ indicated discrepancies attributable to inaccuracy in published line positions. By accurate calibration of the DFWM spectra the absolute frequencies of only clearly resolved transitions were measured and used to derive the improved values for the molecular constants which are presented here. Using these new constants the transition frequencies for the entire band were recalculated and used to construct a synthetic spectrum. The importance of accurate transition frequencies for unresolved components of blended spectral lines is discussed in the context of simulating complex molecular spectra generated by DFWM.

II. EXPERIMENT

The experimental lay-out is illustrated schematically in Fig. 1. C_2 was produced in an oxy-acetylene flame from a standard welding torch. The torch was supplied with industrial grade oxygen and acetylene, and was operated slightly fuel rich to increase the C_2 concentration. The Swan ($d^3\Pi_g-a^3\Pi_u$) system of C_2 was probed using a multimode scanning dye laser (Spectra Physics PDL3) with a linewidth of just under 0.1 cm^{-1} . The dye laser was pumped, at a repetition rate of 10 Hz, with the frequency tripled output of a Q-switched Nd:YAG laser (Spectron Lasers, SL404G) which produced 55 mJ per pulse of 355 nm light (~ 5 ns duration). The dye laser output was attenuated and allowed to propagate over several meters and through several apertures to spatially filter the beam. For the experiments described an overall pulse energy of less than $0.1\text{ }\mu\text{J}$ was used in a uniform beam profile of ~ 2 mm diam in the interaction region. The laser beam was passed through a 70:30 beam-splitter to produce the weak probe beam. The majority of the energy was passed through the interaction region and retro-reflected to form the two counterpropagating pump beams. The weaker probe beam was passed through a second 50:50 beam splitter and directed to cross the pump beams in the interaction region at a small angle ($\sim 1^\circ$). All beam polarizations were linear and parallel. The signal, which travels in a

counterpropagating direction to the probe, was reflected by this second beamsplitter and directed through a spatial filter into a photomultiplier tube for detection. The signal was amplified and digitised using a boxcar averager and recorded on a laboratory computer. To ensure that the transitions were only weakly saturated, several spectra were recorded at different input laser intensities. Analysis of the variation in signal level with incident intensity yielded a value of $I/I_s \sim 0.03$ for the data presented later where I is the incident laser intensity and I_s is the line center saturation intensity.

Wavelength calibration was performed using a Fizeau interferometer system (Lambdameter LM-007). This device consists of four interferometers of varying width incorporated in a temperature stabilised single block. Light entering the device is split and passed through all of the interferometers with the interferograms recorded electronically and analyzed to give a vacuum wavelength reading with a precision up to 1×10^{-5} nm. The calibration of the interferometer system was checked using a single-mode diode laser locked to one of the hyperfine transitions of the caesium D_2 line. With a multimode laser input, the linewidth of the laser is much larger than the precision to which the wavelength reading is given. The analysis of the interferograms attempted to fit the central wavelength from the laser spectrum; where it was unable to do this an error was returned and the data point rejected. One laboratory computer simultaneously recorded the wavelength reading and signal level for each laser pulse and controlled the scanning of the dye laser. The $(0-0)$ band of the ($d^3\Pi_g-a^3\Pi_u$) system of C_2 was recorded in several sections from 512.5 nm to the bandhead at 516.67 nm with the dye laser being stepped across the transitions in steps of 0.0002 nm, taking 20 useful laser shots at each point.

III. CALCULATION OF TRANSITION FREQUENCIES

The experimental values of all the clearly-resolved transition wavelengths were taken from the recorded spectra. A Lorentzian was fitted to each peak, to provide the most accurate measurement of the line center. Although the Abrams and Lind model^{14,15} predicts a Lorentzian cubed line shape this applies only to the case of monochromatic lasers with stationary atoms. In the case where the transition is both homogeneously and inhomogeneously (Doppler) broadened the line shape is more complex and the situation is further complicated by use of a finite bandwidth laser. In practice a simple Lorentzian provided a good fit to the recorded line shapes. Where the spectral lines had a distinct peak but were only closely separated from adjacent transitions, these were fitted simultaneously. Where peaks in the spectrum came from two or more blended transitions, their wavelengths were not used in the subsequent spectral calculation. A number of transitions were present in several of the spectral scans, and the variation in their measured peaks gave an estimated error of 0.003 cm^{-1} .

The band studied is the $(0-0)$ vibrational band of the $d^3\Pi_g-a^3\Pi_u$ electronic transition of the C_2 radical. Both $^3\Pi$ states correspond to Hund's case (a) coupling for the low J rotational levels, but rapidly switch to approximate Hund's case (b) for the higher J levels. Three strong P and R branches are observed, corresponding to transitions between

the F_1 , F_2 , and F_3 spin components. Weaker Q branches are also present, but were not observed in the present study. Some spectroscopic studies of the C_2 radical, such as those of Curtis and Sarre,¹⁶ and Suzuki *et al.*,¹⁷ have also detected satellite transitions between different F spin components, where $\Delta\Omega = \pm 1$. Again these were not seen in this work.

^{12}C is by far the most naturally abundant isotope of carbon. Owing to this, and the quadratic dependence of the degenerate four-wave mixing signal strength on molecular concentration, transitions from $^{12}C_2$ completely dominated the spectra recorded, with no discernible contributions from other isotopes. $^{12}C_2$ is a homonuclear diatomic molecule with a nuclear spin I for both atoms of zero, which results in the absence of all the antisymmetric energy levels. For the $^3\Pi$ states, there is a small energy difference for the two Λ components, which possess opposite parity. Therefore because of the zero nuclear spin, one of these Λ -doublets is missing for each J with the missing component alternating with increasing J . This results in a slight staggering of the separations between transitions in both the P and R branches. The P_1 , P_2 , and P_3 lines form a triplet where, for higher J , the P_1/P_2 components appear as a closely spaced doublet. The staggering of the separations in both P and R branches results in this P_1/P_2 doublet alternating between being separated and strongly blended.

The wave numbers of all the distinct transitions recorded in the experimental scans (about 140 in all) were used in a least-squares fit to calculate molecular constants for the $^3\Pi$ states. The constants required were T , the relative energy of the electronic and vibrational state, B and D , the usual rotational constants, o , p , and q which are λ -doubling coefficients, the spin-coupling constants A and λ with H , A_D , o_D , p_D , and q_D which are centrifugal correction terms. The fit was made using the N^2 Hamiltonian of Brown and Merer for $^3\Pi$ states,¹⁸ with the initial values for the constants taken as those reported by Prasad and Bernath.¹³ Because of the absence of any satellite transitions in the fitted data for which $\Delta\Omega \neq 0$, some of these constants can only be poorly determined. For the fitting to the experimental transition frequencies, the parameters A , H , o , p , o_D , p_D and q_D for the lower energy state, and H , o_D and p_D for the upper state were fixed to the values given by Prasad and Bernath. These were, at most, weakly dependent on the set of transition wavelengths used in the reduction. All the other parameters, however, were varied to achieve a good fit to the experimental positions. The subsequently recalculated values for the transitions, in vacuum wave numbers, are given in Table I. The numbers in parentheses are the difference between calculated and observed wavelengths $(\nu_{\text{calc}} - \nu_{\text{obs}}) \times 10^4$ in cm^{-1} . Where there is no parentheses then the transitions were not sufficiently isolated to be measured or were not observed. A number of the experimental transition frequencies for high J were significantly displaced from the expected values, this is due to the presence of perturbations, most probably in the upper $d^3\Pi_g$ state. The transitions that were not included in the fit to obtain the molecular parameters are indicated in the table and the difference between calculated and observed values are also given.

The values of the molecular parameters obtained from

the fit to the experimental line positions are given in Table II. They are given in the form of the parameters used in the fit, some of which are a combination of a number of the individual constants. The individual values can easily be calculated from these combinations. The errors quoted for the parameters that were varied are given in parentheses and are equal to one standard deviation in units of the last quoted digit. The table lists the molecular parameters for the lower $a^3\Pi_u$ level, and then the difference between the upper state and lower state values, $(X(d^3\Pi_g) - X(a^3\Pi_u))$.

The standard deviation of the difference between calculated and observed values for the fitted transitions came to $3.4 \times 10^{-3} \text{ cm}^{-1}$ which is reasonably consistent with the errors calculated for the measured values. If the calculated transition wavelengths of Prasad and Bernath are used instead, then the standard deviation in the difference of calculated and observed values comes to $7.47 \times 10^{-3} \text{ cm}^{-1}$. While this is only approximately a factor of 2 greater, the differences in the calculated transition wavelengths are substantially different in a number of ways which are important for subsequent simulation of experimental spectra. This is clearly illustrated in Figs. 2 and 3. Figure 2 shows the difference in experimental and calculated values $(\nu_{\text{obs}} - \nu_{\text{calc}})$ for the fitted transitions from the P_1 , P_2 , and P_3 branches. Figure 3 plots the same quantity but using calculated transition positions quoted by Prasad and Bernath instead. Comparison of these two figures shows that the newer calculated positions are closer to the experimental values than those given by Prasad and Bernath, and these latter values become increasingly inaccurate for higher J . In addition, the differences between the calculated values of Prasad and Bernath, and the experimental values show a systematic difference between the separate P branches. This will lead to consistently incorrect separations between neighboring lines from different branches. These separations, especially between the doublets from the P_1 and P_2 branches, are important because they affect the overlap of such closely separated lines. An inaccurate value for the separations and therefore the overlap, leads to poor simulations of experimental degenerate four-wave mixing spectra. This will be illustrated more clearly in the following section. Similar results to this were also obtained using the calculated and experimental values for the R branch transitions.

IV. SIMULATION OF EXPERIMENTAL DFWM SPECTRA

Experimental spectra were both simulated and fitted using a theoretical expression for the DFWM signal level. The computer program used for the spectral simulation is based on the theoretical expression given by Bratfalean *et al.*¹⁹ This gives the electric field strength, E , from the four-wave mixing process for an electronic transition of an ensemble of molecules illuminated with monochromatic light of arbitrary intensity in both pump and probe beams with all input beams linearly and parallel polarized. It does not consider the effect of motion of the atoms. In the limit of a weak probe beam, as was used for this experiment, the expression is approximated by that given by Abrams and Lind^{14,15} for small absorption and reflectivity, where the electric field, E , can be written as

TABLE I. Calculated vacuum wave numbers (in cm^{-1}) for the rotational lines of the swan $d^3\Pi_g-a^3\Pi_u$ (0-0) band of C_2 .^a

J	$P_1(J)$	$P_2(J)$	$P_3(J)$	$R_1(J)$	$R_2(J)$	$R_3(J)$
0						19381.7715
1			19373.6715		19385.1531	19386.5453
2		19372.3420	19370.1645	19388.9705	19389.1623	19391.0409
3	19371.7552	19369.6645	19367.2364	19392.5166	19393.3015	19396.1500
4	19369.3127	19367.0376	19364.6239	19396.3589	19397.8976	19400.9565
5	19367.0174	19364.7923	19362.4699(-21)	19400.4849(-46)	19402.6181(70)	19406.3651(-34)
6	19364.8766	19362.6701(8)	19360.5113(-24)	19404.9140(10)	19407.6781(27)	19411.5649(-41)
7	19362.9407	19360.9201(68)	19358.9681(-40)	19409.6310(-29)	19412.9050(-70)	19417.3361(25)
8	19361.1935(-47)	19359.3137(46)	19357.5595(-66)	19414.6187(50)	19418.4098(12)	19422.9721(-27)
9	19359.6913(3)	19358.0608	19356.5546	19419.9054(-33)	19424.1150(19)	19429.1543(7)
10	19358.3868(34)	19356.9584	19355.6580	19425.4175(-11)	19430.0768(-28)	19435.2438(20)
11	19357.3565	19356.1945	19355.1639	19431.2528(-3)	19436.2512(-15)	19441.8664(19)
12	19356.5150	19355.5907	19354.7633	19437.2645(9)	19442.6837(-37)	19448.4155(6)
13	19355.9747	19355.3101	19354.7704	19443.6334(2)	19449.3229(9)	19455.4964(58)
14	19355.6035	19355.2043	19354.8579(47)	19450.1284(14)	19456.2358(-16)	19462.5066(22)
15	19355.5624	19355.4030	19355.3633	19457.0214(22)	19463.3366(-8)	19470.0569(15)
16	19355.6633	19355.7967(-73)	19355.9343	19463.9888(24)	19470.7364(-26)	19477.5274(-1)
17	19356.1263(13)	19356.4718(58)	19356.9378	19471.3996(-25)	19478.2958(-10)	19485.5545(31)
18	19356.6991(-7)	19357.3672	19357.9889(64)	19478.8316(21)	19486.1866(-23)	19493.4833(27)
19	19357.6695(-53)	19358.5163(-35)	19359.4918(21)	19486.7562(56)	19494.2015(-23)	19501.9922(5)
20	19358.7131(-13)	19359.9155(-15)	19361.0202(-18)	19494.6470(50)	19502.5861(-49)	19510.3769(7)
21	19360.1928(22)	19361.5364(-36)	19363.0239(26)	19503.0825(15)	19511.0534(-110)	19519.3709
22	19361.7057(-5)	19363.4414(25)	19365.0272(-9)	19511.4272(11)	19519.9337	19528.2088
23	19363.6964(3)	19365.5321(-34)	19367.5333(17)	19520.3716	19528.8502	19537.6902
24	19365.6770(-14)	19367.9447(-6)	19370.0095(0)	19529.1661	19538.2272	19546.9785
25	19368.1800(-5)	19370.5032(30)	19373.0193(15)	19538.6177	19547.5898	19556.9487
26	19370.6265(-28)	19373.4249(17)	19375.9663(25)	19547.8583	19557.4642	19566.6845
27	19373.6428(-19)	19376.4493(31)	19379.4812(39)	19557.8157	19567.2699	19577.1445
28	19376.5537(-21)	19379.8814(12)	19382.8971(-15)	19567.4989	19577.6419	19587.3247
29	19380.0840(20)	19383.3699(44)	19386.9182(-15)	19577.9607	19587.8875	19598.2749
30	19383.4577(-10)	19387.3136(-19)	19390.8010(-39)	19588.0834	19598.7570	19608.8966
31	19387.5025(-35)	19391.2644(83)	19395.3291(13)	19599.0483	19609.4396	19620.3371
32	19391.3375(-21)	19395.7202(58)	19399.6772(2)	19609.6074	19620.8061	19631.3972
33	19395.8971(9)	19400.1316	19404.7129(2)	19621.0738	19631.9226	19643.3275
34	19400.1918	19405.1003(46)	19409.5245(18)	19632.0666	19643.7854	19654.8233
35	19405.2663(-22)	19409.9706	19415.0681(-13)	19644.0328	19655.3331	19667.2426
36	19410.0194	19415.4523(37)	19420.3416(-8)	19655.4564	19667.6910	19679.1711
37	19415.6086(-6)	19420.7799	19426.3932(-85)	19667.9207	19679.6669	19692.0784
38	19420.8187	19426.7746(8)	19432.1270(-40)	19679.7724	19692.5186	19704.4369
39	19426.9221(-56)	19432.5580	19438.6863(-44)	19692.7329	19704.9201	19717.8307
40	19432.5880	19439.0653(-2)	19444.8789(-24)	19705.0102	19718.2639	19730.6165
41	19439.2050(-8)	19445.3031	19451.9454(-41)	19718.4644	19731.0882	19744.4949
42	19445.3253	19452.3225(22)	19458.5954(-33)	19731.1649	19744.9221	19757.7054
43	19452.4549(-20)	19459.0133	19466.1683(-4)	19745.1104	19758.1667	19772.0663
44	19459.0287	19466.5438(63)	19473.2744(57)	19758.2317	19772.4884	19785.6989
45	19466.6695(43)	19473.6863	19481.3525(268) ^b	19772.6657	19786.1507	19800.5399
46	19473.6958	19481.7266(340) ^b	19488.9134(-30) ^b	19786.2055	19800.9575	19814.5922
47	19481.8461(369) ^b	19489.3197	19497.4952	19801.1249	19815.0353	19829.9103
48	19489.3240	19497.8683	19505.5098(-1269) ^b	19815.0812	19830.3242	19844.3800
49	19497.9821	19505.9108	19514.5935	19830.4824	19844.8151	19860.1721
50	19505.9107	19514.9658	19523.0607	19844.8532	19860.5827	19875.0568

^aThe number in parentheses indicates $(\nu_{\text{calc}} - \nu_{\text{obs}}) \times 10^4$ in cm^{-1} .^bIndicates lines not used in the fit to calculate the molecular parameters.

$$E = \sum_n \frac{|\mu_n|^2 \Delta N_n T_{2n} k_n L (1 - i \delta_n)}{2 \epsilon_0 \hbar (1 + \delta_n^2)} \times \frac{2 I_{pu} \sqrt{I_{pr}/I_{sn}} (1 + \delta_n^2)}{[1 + 4 I_{pu}/I_{sn} (1 + \delta_n^2)]^{3/2}}$$

This contains a summation over all transitions n where μ_n is the electric dipole moment, ΔN_n the population difference between ground and upper state, k_n the wave vector, and T_{1n}

and T_{2n} the longitudinal and transverse relaxation times for that transition. δ_n is the normalized detuning for the transition, given by $\delta_n = (\omega - \omega_{0n}) T_{2n}$ with ω_{0n} the transition line center. I_{sn} is the line center saturation intensity for the transition, $I_{sn} = \hbar^2 / (T_{1n} T_{2n} |\mu_n|^2)$. L is the length of the interaction region, and I_{pu} and I_{pr} the pump and probe beam intensities, respectively.

A monochromatic spectrum was simulated by adding the

TABLE II. Molecular parameters (in cm^{-1}) for the $a^3\Pi_u$ state of C_2 and the difference between the upper $d^3\Pi_g$ state and lower $a^3\Pi_u$ state.

Parameter	$a^3\Pi_u$	$(d^3\Pi_g)-(a^3\Pi_u)$
T	0.0	19378.46456(72)
B	1.624075(30)	0.1215293(24)
$D \times 10^6$	6.479(35)	0.3760(31)
$A_D \times 10^4$	2.76(73)	2.66(15)
A	-15.2696 ^a	1.2691(18)
$H \times 10^{12}$	7.85 ^a	-7.85 ^a
$o+p+q$	0.67726 ^a	-0.06460(87)
$p+2q \times 10^3$	1.408 ^a	1.010(36)
$q \times 10^4$	-4.97(21)	-2.666(26)
$o_D+p_D+q_D \times 10^6$	-8.122 ^a	8.122 ^a
$p_D+2q_D \times 10^8$	9.42 ^a	-0.942 ^a
$q_D \times 10^8$	-1.288	2.49(19)
λ	-0.1476(55)	0.1786(10)

^aIndicates parameters fixed to the values of Prasad and Bernath (Ref. 13).

signal field at a frequency ω from all transitions in the spectrum with the correct phase and taking $|E|^2$ to give the signal intensity at that frequency. A negligible population was assumed in the upper state, and the ground state populations were assumed to follow a Boltzmann distribution such that $\Delta N_n \propto (2J_n + 1) \exp(-E_n/k_B T)$ with E_n the ground state energy, J_n the total angular momentum, and T the temperature. The simulation assumed equal relaxation rates for all the transitions which were observed, $T_{1n} = T_1$, $T_{2n} = T_2$, and the relative dipole moments μ_n and ground state energies E_n were calculated by the program that was used for fitting and calculation of the transition frequencies ω_{0n} . The effect of the variation of degeneracy of the levels involved in the transitions was also incorporated. J dependent geometrical factors have been derived by Williams *et al.*²⁰ for the different rotational branches and for different geometries to account for variation in signal level owing to such factors. The signal field was also multiplied by the geometrical factor G_F given by Williams *et al.*²⁰

The laser used was not monochromatic but had a bandwidth wider than that of the transitions. A time averaged measurement of the laser spectral profile was obtained by

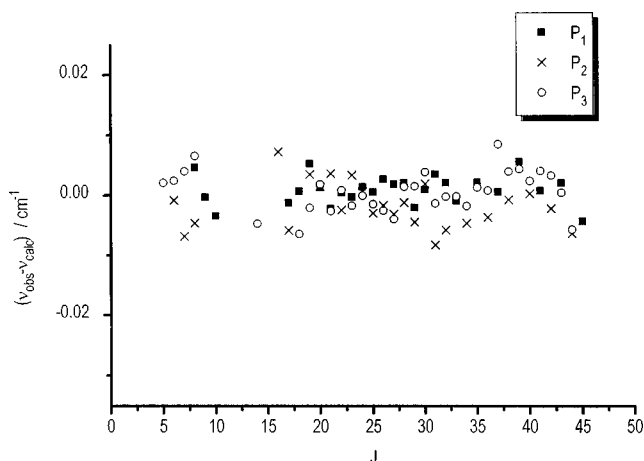


FIG. 2. Difference between experimentally measured and calculated line positions for the P branches, using the calculated values presented in this paper.

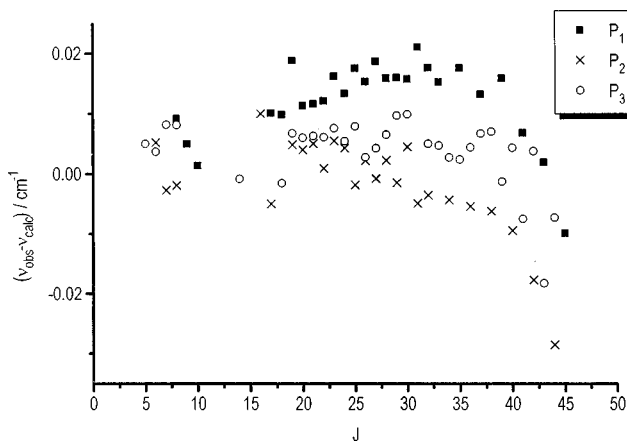


FIG. 3. Difference between experimentally measured and calculated line positions for the P branches, using the calculated values given by Prasad and Bernath.

passing the laser through a Fabry-Perot étalon and scanning the dye laser through several free spectral ranges. The spectral profile was found to be well approximated by a Gaussian of width (FWHM) 0.090 cm^{-1} . To simulate the effect of this finite bandwidth on the measured spectra, the theoretical monochromatic spectrum was convolved with a Gaussian of width $0.090/\sqrt{3} = 0.053 \text{ cm}^{-1}$. The factor of $\sqrt{3}$ comes from the cubic dependence of the signal intensity on the input laser intensity, in the unsaturated regime. With a finite laser bandwidth, there will also be contributions to the signal from nearly degenerate four-wave mixing, particularly when the motion of the molecules is taken into account. These however were not included in these simulations.

This simulation method which has been outlined is based on a theory which deals only with the effects of molecular motion in the forward geometry with small crossing angles and not in the phase-conjugate geometry as was used in the present work. It also only compensates for the finite bandwidth of the input lasers in a simple manner. In addition, crossover resonances are not included although these do not occur in this spectral region of C_2 . As the input intensities were weak the effects of molecular motion and finite bandwidth, including nearly-degenerate four wave mixing, can be calculated by perturbative means, but such additional calculation is computationally expensive. The simulation and fitting of experimental spectra on an ordinary PC would not be feasible in a realistic time scale with such additional analysis. The high quality of agreement between our final simulations and the experimental data justifies the neglect of these additional factors in these circumstances. Finite bandwidth effects will be more important, however, when saturation occurs, especially with larger bandwidth input fields. Molecular motion would also significantly alter the spectral line shape in the case where the input laser bandwidth is much less than the Doppler width.

An important parameter for the correct simulation of complex rotational spectra is the homogeneous linewidth of the transitions, which in the theoretical approach used here is governed by the transverse relaxation time T_2 . Few publications give any indication of the homogeneous linewidth for

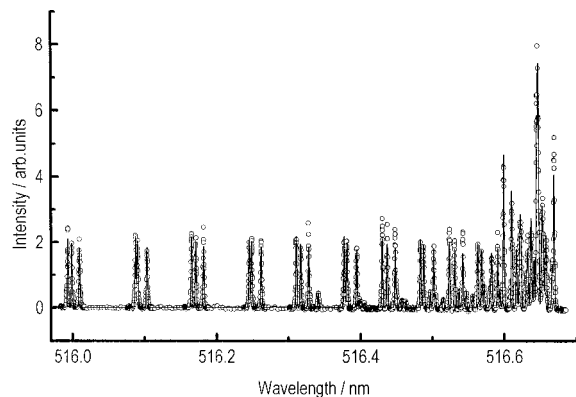


FIG. 4. Experimental spectrum and theoretical fit to the bandhead region of the Swan (0-0) band of C_2 . Open circles, experimental data; solid line, theoretical simulation.

the C_2 molecule in an atmospheric pressure flame, and those values that are quoted show some disagreement. The value of T_2 used for these simulations was obtained by fitting a theoretical spectrum to an appropriate section of the C_2 experimental spectrum. Where many rotational transitions exist within a small spectral range, the overlap, and therefore the intensity, of the spectral feature is strongly dependent on the intrinsic transition linewidth. The ratio of the intensities of such blended features to isolated transitions is therefore changed substantially by variation in the linewidth. This effect is most evident around the bandhead region, and so a value of T_2 was obtained by fitting the spectral region from 516 nm onwards which contains both the bandhead and many isolated P branch transitions. Only a small range of T_2 values enabled both isolated and blended features to be simultaneously fitted. The whole region was fitted with T_2 as an adjustable variable to obtain a value of 0.161 ns, which corresponds to a homogeneous linewidth of 0.066 cm^{-1} . The spectrum was also fitted using the line positions given by Prasad and Bernath to obtain a value of $T_2 = 0.156\text{ ns}$. This value is very similar to that obtained with the newly calculated transition frequencies indicating that such a derivation of T_2 is fairly insensitive to the exact transition wavelengths. Figure 4 shows the experimental spectra and theoretical fit to this bandhead region, showing the high quality of the simulation in this complex spectral region. In all these simulations the temperature was fixed to 3000 K. This is the average temperature previously measured in this flame using degenerate four-wave mixing^{9,10} and is similar to the value calculated and measured by other optical means for such a flame.²¹ The bandhead spectrum is, in any case, fairly insensitive to variations in the temperature.

Figure 5 shows a smaller section of this bandhead spectrum with the theoretical simulation. For comparison, the fits of a theoretical simulation using the transition wavelengths given by Prasad and Bernath,¹³ and also those given by Amiot¹² are also shown. Although the bandhead spectra are less sensitive to the precise line positions than many other parts of the C_2 Swan (0-0) band, it is clear from Fig. 5 that the best simulation is obtained using the line positions presented in this paper. This is despite the fact that very few

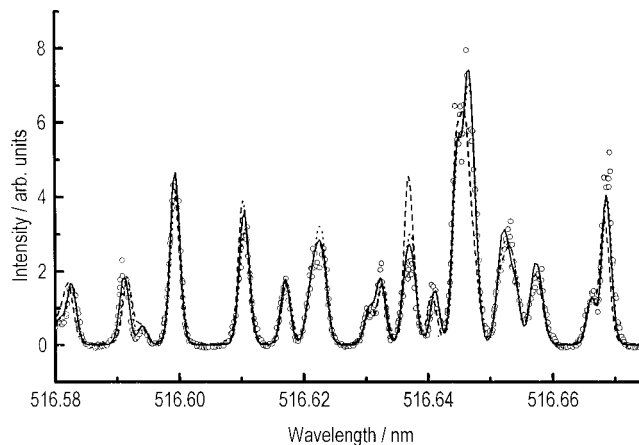


FIG. 5. Enlargement of bandhead region with simulations using different line positions. Open circles, experimental data. Simulations are shown using line positions from this work, solid line; Amiot, long dash; Prasad and Bernath, short dash.

isolated lines exist in the bandhead region, and so few lines from these spectra were included in the data used to calculate the new molecular parameters. This improvement in fitting is confirmed by the quality of fit factor used for fitting the simulations to the experimental data, which consisted of the sum of the squares of the residue between theory and experimental data. For the whole bandhead region as shown in Fig. 4, this factor was 65% larger when using the Prasad and Bernath line positions and over three times greater with those given by Amiot.

The importance of accurate line positions for spectral simulation is most evident in regions of the spectrum where the separation of P_1/P_2 doublets approaches the homogeneous width. Alternate doublets then become strongly blended and the effects of coherent addition are seen in the resulting spectral line intensity. This is illustrated in Fig. 6 which shows four spectra of such a region between 515 and 516 nm. Figure 6(a) shows the experimental spectrum in which the P_1/P_2 components lie to the short wavelength side of the triplets. For most of the spectrum these doublets do not overlap and no increase in signal arises from coherent addition. Only at the low wavelength end of the region plotted does such an effect occur. The other three diagrams of Fig. 6 are simulated spectra which have been fitted to the experimental data using the line positions presented in this work, those of Prasad and Bernath and finally those of Amiot. Using the previously published line positions the P_1/P_2 doublet separations are wrong and in the alternate doublets, which are more closely separated, the simulations predict overlap and a subsequent increase in signal level where this is not observed experimentally. For the P triplet marked with an arrow in Fig. 6, for example, the ratio of the P_1/P_2 doublet peak height to that of the neighboring isolated P_3 transition is approximately 1.80 for the experimental spectrum, 1.94 for the simulation using the new line positions, 2.68 using those of Prasad and Bernath, and 4.24 with Amiot's. Use of these less accurate line positions makes it very difficult to simulate such a spectral region well. This is again indicated by a dramatic increase (at least three times

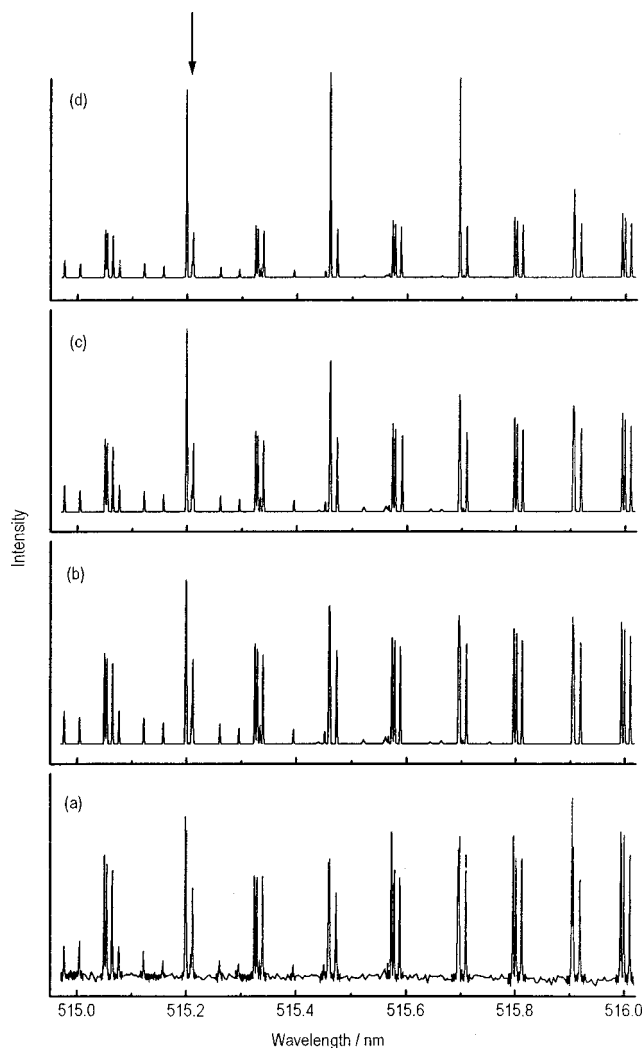


FIG. 6. Part of the spectrum of the Swan (0-0) band of C_2 illustrating the effect on relative line intensities of inaccuracies in line positions used in simulating blended features. (a) Experimental data (this work). Simulation using line positions given by (b) this work, (c) Prasad and Bernath, (d) Amiot.

larger) in the square of the residue between simulation and experimental data using these previous transition wavelengths compared to the newly calculated values.

V. CONCLUSION

High resolution spectra have been taken of the Swan $d^3\Pi_g - a^3\Pi_u(0-0)$ band of C_2 , using degenerate four-wave mixing. The conditions of the experiment were not the most favorable for high resolution spectroscopy. The source was at atmospheric pressure and so suffered substantial pressure broadening and was also at high temperature giving a large Doppler width to the transitions. In addition a laser with narrower linewidth than the multimode laser from the present work could be used. Despite these factors, a resolution was achieved which was sufficient to resolve some well-blended doublets which had not been resolved in any other previously reported spectroscopic measurements of this vibrational branch. This indicates the utility of nonlinear laser-based methods such as degenerate four-wave mixing for high

resolution spectroscopy. This is particularly so for molecular species which are short-lived or are produced only in hostile environments. Degenerate four-wave mixing in the phase conjugate geometry, as was used for these experiments, is a sub-Doppler technique. The cubic dependence of signal strength on incoming nonsaturating laser intensities can also lead to a measured transition width less than that of the probing laser. In addition the contribution to the measured linewidth from the homogeneous width of the transition is also less because of the nonlinear nature of the process. A truly monochromatic nonsaturating input laser would measure a linewidth of less than half that obtained using linear techniques, with a subsequent increase in resolution. All these factors contribute to the high resolution possible with DFWM as demonstrated here.

The transition wavelengths measured from the experimental spectra were used to recalculate molecular parameters for the $a^3\Pi_u$, $\nu=0$ and $d^3\Pi_g$, $\nu=0$ states. These were then used to calculate transition wavelengths for the whole band. A comparison of the newly calculated wavelengths with the those observed experimentally, showed substantially greater agreement than with the line positions reported in earlier works. In particular, a systematic movement of all transitions in one branch with respect to those in another which could clearly be seen from previous published wavelength data was removed. This is important in providing more accurate values for the separation of near-neighboring transitions. It is hoped that these new line positions will be beneficial in future work where simulation of this band of the C_2 radical is required.

The importance of accurate knowledge of line positions in simulating spectra using nonlinear processes such as degenerate four-wave mixing was illustrated. Experimental spectra from different regions of the Swan $d^3\Pi - a^3\Pi(0-0)$ band of C_2 were simulated and fitted using the line positions presented here and also from two previous spectroscopic studies of this band. In all regions of the spectrum better fits were obtained with the new line positions because features containing overlapping transitions were calculated to have the correct intensity in comparison to isolated transitions. Where spectroscopic techniques such as DFWM are used for diagnostic measurements, great importance is often attached to the variation in intensity of spectral features or the ratio in intensities of different features. The work presented here demonstrates that a sufficiently accurate knowledge of the spectral line positions will at times be necessary to obtain correct results from such measurements.

ACKNOWLEDGMENTS

The authors like to thank Professor John Brown for his substantial help and the use of the computer program HUNDA used for deriving the molecular parameters and line positions of C_2 given in this paper. We are grateful to the EPSRC for their financial support of this research.

¹P. Ewart and S. V. O'Leary, *Opt. Lett.* **11**, 279 (1986).

²K. Nyholm, R. Maier, C. G. Aminoff, and M. Kaivola, *Appl. Opt.* **32**, 919 (1993).

³R. L. Farrow and D. J. Rakestraw, *Science* **257**, 1894 (1992).

- ⁴P. H. Vaccaro, in *Nonlinear Spectroscopy for Molecular Structure Determination*, edited by E. Hirota, R. W. Field, J. P. Maier, and S. Tsuchiya (Blackwell, London, 1997).
- ⁵M. Aldén, H. Edner, and S. Svanberg, *Appl. Phys. B: Photophys. Laser Chem.* **29**, 93 (1982).
- ⁶A. P. Baronavski and J. R. McDonald, *Appl. Opt.* **16**, 1897 (1977).
- ⁷C. F. Kaminski and P. Ewart, *Appl. Phys. B: Lasers Opt.* **61**, 585 (1995).
- ⁸K. Nyholm, M. Kaivola, and C. G. Aminoff, *Appl. Phys. B: Lasers Opt.* **60**, 5 (1995).
- ⁹C. F. Kaminski, I. G. Hughes, G. M. Lloyd, and P. Ewart, *Appl. Phys. B: Lasers Opt.* **62**, 39 (1996).
- ¹⁰C. F. Kaminski, I. G. Hughes, and P. Ewart, *J. Chem. Phys.* **106**, 5324 (1997).
- ¹¹R. T. Bratfalean, G. M. Lloyd, and P. Ewart (to be published).
- ¹²C. Amiot, *Astrophys. J., Suppl. Ser.* **52**, 329 (1983).
- ¹³C. V. V. Prasad and P. F. Bernath, *Astrophys. J.* **426**, 812 (1994).
- ¹⁴R. L. Abrams and R. C. Lind, *Opt. Lett.* **2**, 94 (1978).
- ¹⁵R. L. Abrams and R. C. Lind, *Opt. Lett.* **3**, 205 (1978).
- ¹⁶C. M. Curtis and P. J. Sarre, *J. Mol. Spectrosc.* **114**, 427 (1985).
- ¹⁷T. Suzuki, S. Saito, and E. Hirota, *J. Mol. Spectrosc.* **113**, 399 (1985).
- ¹⁸J. M. Brown and A. J. Merer, *J. Mol. Spectrosc.* **74**, 488 (1979).
- ¹⁹R. T. Bratfalean, G. M. Lloyd, and P. Ewart (submitted).
- ²⁰S. Williams, R. N. Zare, and L. A. Rahn, *J. Chem. Phys.* **101**, 1072 (1994).
- ²¹B. Lewis and G. von Elbe, *Combustion, Flame and Explosion of Gases*, 2nd ed. (Academic, New York, 1961).